

RESEARCH LETTER

10.1002/2018GL077536

Key Points:

- Large regional differences exist in wetland methane isotopic source signatures
- Spatially resolved methane isotope signatures are critical for simulating atmospheric variability
- Biases will result in atmospheric inversions if spatial patterns are not accounted for in methane isotope source signatures

Supporting Information:

- Supporting Information S1
- Data Set S1

Correspondence to:

A. L. Ganesan,
anita.ganesan@bristol.ac.uk

Citation:

Ganesan, A. L., Stell, A. C., Gedney, N., Comyn-Platt, E., Hayman, G., Rigby, M., et al. (2018). Spatially resolved isotopic source signatures of wetland methane emissions. *Geophysical Research Letters*, 45, 3737–3745. <https://doi.org/10.1002/2018GL077536>

Received 9 FEB 2018

Accepted 24 MAR 2018

Accepted article online 30 MAR 2018








Published online 21 APR 2018

The copyright line for this article was changed on 27 APR 2018 after original online publication.

©2018. The Authors.

This is an open access article under the terms of the Creative Commons Attribution License, which permits use, distribution and reproduction in any medium, provided the original work is properly cited.

Spatially Resolved Isotopic Source Signatures of Wetland Methane Emissions

A. L. Ganesan¹ , A. C. Stell² , N. Gedney³, E. Comyn-Platt⁴ , G. Hayman⁴ , M. Rigby² , B. Poulter⁵ , and E. R. C. Hornibrook⁶ 

¹School of Geographical Sciences, University of Bristol, Bristol, UK, ²School of Chemistry, University of Bristol, Bristol, UK, ³Met Office, Hadley Centre, Joint Centre for Hydrometeorological Research, Wallingford, UK, ⁴Centre for Ecology and Hydrology, Wallingford, UK, ⁵NASA Goddard Space Flight Center, Biospheric Sciences Laboratory, Greenbelt, MD, USA, ⁶Department of Earth, Environmental and Geographic Sciences, The University of British Columbia, Okanagan Campus, Kelowna, British Columbia, Canada

Abstract We present the first spatially resolved wetland $\delta^{13}\text{C}(\text{CH}_4)$ source signature map based on data characterizing wetland ecosystems and demonstrate good agreement with wetland signatures derived from atmospheric observations. The source signature map resolves a latitudinal difference of $\sim 10\text{‰}$ between northern high-latitude (mean -67.8‰) and tropical (mean -56.7‰) wetlands and shows significant regional variations on top of the latitudinal gradient. We assess the errors in inverse modeling studies aiming to separate CH_4 sources and sinks by comparing atmospheric $\delta^{13}\text{C}(\text{CH}_4)$ derived using our spatially resolved map against the common assumption of globally uniform wetland $\delta^{13}\text{C}(\text{CH}_4)$ signature. We find a larger interhemispheric gradient, a larger high-latitude seasonal cycle, and smaller trend over the period 2000–2012. The implication is that erroneous CH_4 fluxes would be derived to compensate for the biases imposed by not utilizing spatially resolved signatures for the largest source of CH_4 emissions. These biases are significant when compared to the size of observed signals.

Plain Language Summary Concentrations of methane are increasing in the atmosphere. In order to understand the reasons behind such variations, carbon isotopes are used to help identify changes in emission sources and sinks. We present a new global map of the carbon isotope signature associated with wetland methane emissions, the largest global source of methane to the atmosphere. We show how this newly synthesized information can lead to more accurate understanding of the causes of variations in the amount and rate of increase of methane in the atmosphere.

1. Introduction

Methane (CH_4) is the second most important greenhouse gas after carbon dioxide and is emitted from a variety of natural and anthropogenic sources (Saunio et al., 2016). Natural wetlands are the single largest individual source of CH_4 emissions to the atmosphere, which can vary significantly in time and space due to environmental factors such as temperature and precipitation. Numerous studies have quantified wetland CH_4 emissions through both bottom-up and top-down approaches, often with large disparity, particularly on regional scales (Saunio et al., 2016).

The rate of increase of CH_4 in the atmosphere exhibits strong year-to-year changes due to variations in the strengths of sources and sinks (Saunio et al., 2016). In the 1980s, the CH_4 growth rate was $> 10 \text{ ppb yr}^{-1}$, then after 1992, was approximately zero and again resumed at about 6 ppb yr^{-1} after 2007 (Nisbet et al., 2016). Diagnosing the mechanisms behind these fluctuations continues to generate considerable attention and controversy, in particular for the period after 2007, when CH_4 concentrations began to rise globally after a decade of near stability (Dlugokencky et al., 2009; Nisbet et al., 2016; Rigby et al., 2008). Explanations proposed for the post-2007 rise include increases in tropical wetland emissions (Nisbet et al., 2016), increases in fossil fuel emissions (Hausmann et al., 2016), increases in agricultural emissions (Schaefer et al., 2016), reduction in biomass burning (Worden et al., 2017), and changes to the main atmospheric sink, the hydroxyl radical (Rigby et al., 2017; Turner et al., 2017). These varying conclusions are largely driven by the same or similar sets of observations: measurements of CH_4 mole fraction and observations of the ^{13}C isotopologue of CH_4 (hereby expressed as $\delta^{13}\text{C}(\text{CH}_4) = ((R_{\text{sample}}/R_{\text{standard}}) - 1)$ where $R = ^{13}\text{C}/^{12}\text{C}$ and the standard is Vienna Peedee Belemnite; Coplen, 2011) at atmospheric monitoring stations around the world. While the

atmospheric mole fraction of CH₄ has increased after 2007, atmospheric δ¹³C(CH₄) has simultaneously decreased (i.e., become more ¹³C-depleted; Nisbet et al., 2016). Measurements of δ¹³C(CH₄) are useful for source attribution because fossil fuel, and biological CH₄ sources have distinctive signatures and sink process partition ¹³CH₄ and ¹²CH₄ to different extents. Accurate characterization of these isotopic “fingerprints” coupled with observations of atmospheric CH₄ and δ¹³C(CH₄) enables the diagnosis of drivers of variability in the growth rate of atmospheric CH₄. However, the accuracy of those diagnoses relies strongly upon accurate characterization of the δ¹³C(CH₄) signatures of emission sources.

Previous studies that have utilized δ¹³C(CH₄) observations to examine drivers of interannual variability have typically employed a globally uniform isotopic source signature for wetlands of approximately –60‰ (Bousquet et al., 2006; Houweling et al., 2000; Mikaloff Fletcher et al., 2004; Monteil et al., 2011; Quay et al., 1999; Rigby et al., 2012). This simplifying assumption has been made mostly due to the lack of a gridded δ¹³C(CH₄) wetland source signature map. A similar approach has been used in studies that analyzed the post-2007 increase in the growth rate of atmospheric CH₄ (Ghosh et al., 2015; Rice et al., 2016; Schaefer et al., 2016; Schwietzke et al., 2016) with the exception of Warwick et al. (2016), who attributed separate δ¹³C(CH₄) signatures to high-latitude and tropical wetlands, and Feinberg et al. (2018), who employed a uniform δ¹³C(CH₄) signature for the tropics and linearly decreasing δ¹³C(CH₄) values for high-latitude wetlands.

Decades of field measurements show that the δ¹³C(CH₄) values of wetland CH₄ emissions are not uniform (Bellisario et al., 1999; Chasar, 2000; Crill et al., 1988; Lansdown et al., 1992; Quay et al., 1988). Northern high-latitude wetlands, which are dominated by ombrotrophic bogs and minerotrophic fens, are the best characterized wetlands globally with respect to CH₄ source strength (Turetsky et al., 2014) and δ¹³C(CH₄) values (Hornibrook, 2009). CH₄ is produced in ombrotrophic bogs primarily via the CO₂/H₂ methanogenesis pathway because low pH limits acetoclastic methanogenesis (Duddleston et al., 2002; Hines et al., 2001), resulting in the production of CH₄ that is highly ¹³C-depleted (Lansdown et al., 1992). In contrast, minerotrophic fens, which receive significant input of groundwater, have a neutral to alkaline pH and greater prevalence of methanogenesis via acetate fermentation, yielding more positive δ¹³C(CH₄) values (Bellisario et al., 1999). Differences in primary δ¹³C(CH₄) compositions (Bellisario et al., 1999; Hornibrook & Bowes, 2007) coupled with predictable distributions of methanogenic pathways (Hornibrook, 2000) and gas transport processes (Chanton, 2005) yield CH₄ emissions with distinctly different δ¹³C(CH₄) values in ombrotrophic bogs (–74.9 ± 9.8‰, *n* = 42) and minerotrophic fens (–64.8 ± 4.0‰, *n* = 38). These values are means and standard deviations from a compilation of field-based chamber studies of δ¹³C(CH₄) flux to the atmosphere (Hornibrook, 2009).

Tropical wetlands are dominated by marshes and swamps (Bartlett & Harriss, 1993) and are less well studied than bogs and fens. There is little distinction in methanogenic metabolism between marshes and swamps; however, differences in tropical δ¹³C(CH₄) source signatures can result from a prevalence of C4 (i.e., Hatch-Slack photosynthetic pathway) plants, which when decomposed anaerobically, produce CH₄ that is markedly ¹³C-enriched (Chanton et al., 1989; Quay et al., 1988; Stevens & Engelkemir, 1988; Tyler et al., 1988). In this study, we use δ¹³C(CH₄) source signatures of –60 ± 4‰ for C3 and –50 ± 4‰ for C4 tropical wetlands, consistent with current literature δ¹³C(CH₄) values for tropical wetlands.

Here we develop a wetland δ¹³C(CH₄) source signature map based on current understanding of key biogeochemical distinctions between wetland types and the source signatures associated with those types as discussed above.

2. Methods

We develop a 0.5° resolution wetland δ¹³C(CH₄) source signature map based on differences in wetland ecosystems. We evaluate the map against independent observations of regional wetland δ¹³C(CH₄) signatures inferred from Keeling plots of atmospheric observations. Using the refined δ¹³C(CH₄) source signature map for wetlands, we assess its potential impact on modeling atmospheric δ¹³C(CH₄) variability, specifically on spatial and seasonal patterns in δ¹³C(CH₄), and trend during the period 2000 to 2012. We show the benefit of using spatially resolved wetland δ¹³C(CH₄) signatures for atmospheric inversion studies by quantifying inaccuracies that would result from using a uniform wetland δ¹³C(CH₄) source signature.

2.1. Distribution of Major Wetland Classes With Distinct Source Signatures

We investigate whether the variability in global wetland source signatures can be captured using four major wetland types: ombrotrophic and minerotrophic wetlands at northern high latitudes (defined as $>45^{\circ}\text{N}$) and C3 and C4 wetlands in the subtropics and tropics (between 40°N and 40°S). Over 95% of ombrotrophic bogs and minerotrophic fens wetlands exist in the northern high latitudes (Matthews & Fung, 1987). In the region between 40° to 45°N and S , we apply a smooth gradient for each band of longitude. Wetlands located south of 45°S were not considered because their area comprises less than 1% of total wetland area globally (Poulter et al., 2017).

To our knowledge, a high-resolution globally consistent data set delineating ombrotrophic and minerotrophic wetlands currently does not exist. Consequently, we define the areal extent of these wetlands via a soil pH proxy. The fraction of ombrotrophic and minerotrophic wetland in each grid cell is computed using the Harmonized World Soil Database v1.1, which contains soil pH data at 30 arc-second resolution (FAO/IIASA/ISRIC/ISSCAS/JRC, 2009). We test a range of pH thresholds (pH 4.5–5.2) to delineate ombrotrophic and minerotrophic wetlands, validating the resulting distributions against observational peatland data from two high-latitude regions in Canada and Western Siberia (Peregon et al., 2009; Tarnocai et al., 2000). A pH of 5 yields the best fit to observational data (supporting information).

In the tropics, we use the C3 and C4 vegetation distribution map from Still et al. (2003), which is based on a combination of remote-sensing, climate modeling, and ground-based data. Extensive validation of the areal extent of C3- and C4-dominated wetlands in the tropics was limited by poor availability of observational data.

2.2. Generation of $\delta^{13}\text{C}(\text{CH}_4)$ Source Signature Map

The fraction of each wetland type within a 0.5° grid cell is weighted by $\delta^{13}\text{C}(\text{CH}_4)$ source signatures associated with those wetlands (section 1) to produce the net $\delta^{13}\text{C}(\text{CH}_4)$ source signature map. The impact of the ranges in $\delta^{13}\text{C}(\text{CH}_4)$ values for each wetland type is investigated further in section 3. Because multiple wetland flux data sets exist (using different wetland areas), the source signature data file provided in the supporting information contains a source signature value for every grid cell globally. It can therefore be used in conjunction with any flux and wetland area data set. In our analyses, we use wetland fluxes defined over the inundated area data set from Poulter et al. (2017). The inundated fraction associated with rice is removed using the monthly climatology rice map from Portmann et al. (2010).

2.3. Validation Against Atmospheric Observations

To provide an independent evaluation of the source signature map, we compare simulated atmospheric $\delta^{13}\text{C}(\text{CH}_4)$ values at several locations against regional source signatures inferred from atmospheric observations. Regional source signatures were inferred through Keeling plots from Brownlow et al. (2017), Fisher et al. (2017), Umezawa et al. (2012), and Umezawa et al. (2011) for Alaska, Canada, Scandinavia, Siberia, Costa Rica, Bolivia, Uganda, South Africa, Borneo, and Hong Kong. There are several requirements that need to be met to infer signatures from Keeling plots (Pataki et al., 2003), and these are discussed in the measurement studies. For this study, it is important that wetlands are the sole source of CH_4 emissions in the regions sampled by the observations. These studies have sampled from regions where wetlands were isolated from other CH_4 emission sources.

The source signatures derived through atmospheric measurements are representative of a larger scale (tens of kilometers) than the chamber measurements from which the signatures for each wetland type have been assigned (meters). Any fine-scale heterogeneity, which would not be represented by the flux model or the transport model, is integrated by the atmosphere. The intention of the source signature map is to simulate regional patterns and not to represent fine-scale heterogeneity.

The simulated atmospheric $\delta^{13}\text{C}(\text{CH}_4)$ at a particular site is the flux and surface sensitivity weighted contributions of source signature from each grid cell in the domain:

$$\delta^{13}\text{C}(\text{CH}_4)_{\text{site}} = \frac{\sum_i f_i \cdot h_i \cdot \delta_i}{\sum_i f_i \cdot h_i} \quad (1)$$

where i is the grid cell, f_i is the $^{12}\text{CH}_4$ flux in $\text{mol m}^{-2} \text{s}^{-1}$, h_i is the surface sensitivity in $(\text{mol/mol})/(\text{mol m}^{-2} \text{s}^{-1})$, and δ_i is the wetland source signature.

The sensitivity of each observation to fluxes from the surface is derived using the Lagrangian Particle Dispersion Model, NAME (Numerical Atmospheric dispersion Modelling Environment). NAME simulates atmospheric transport using three-dimensional meteorological fields from the Unified Model at approximately 17-km resolution (in 2016; the resolution depends on the year the measurements were made). The model output quantifies the relationship between concentration at a measurement location and time, and surface emissions from each grid cell of the regional domain (e.g., Manning et al., 2011). The mean sensitivity over the period that the samples were collected for the Keeling plot analysis is used for h_i in equation (1).

Monthly wetland CH₄ fluxes are estimated from the land-surface model JULES (Joint UK Land Environment Simulator) during the period 2000 to 2012 (Comyn-Platt et al., 2018; Saunois et al., 2016). Because the relative differences in fluxes between different wetlands in the region impacts the calculation of atmospheric $\delta^{13}\text{C}(\text{CH}_4)$, we tune fluxes for bogs and fens based on the comprehensive evaluation in Turetsky et al. (2014; supporting information). A similar tuning is not possible for the tropical wetlands because there are not enough tropical wetland sites with fluxes resolved by C3 and C4 vegetation in the Turetsky et al. (2014) analysis. For the tropics, standard JULES output was used (Comyn-Platt et al., 2018; Saunois et al., 2016).

For each site, we simulate 1,000 $\delta^{13}\text{C}(\text{CH}_4)$ values using randomly drawn samples of the source signature from each wetland type and compare this distribution to the observed $\delta^{13}\text{C}(\text{CH}_4)$. Samples are drawn from a Gaussian distribution with the mean and standard deviation defined by observed values (section 1). The resulting distribution provides an estimate of the uncertainty in the simulated $\delta^{13}\text{C}(\text{CH}_4)$ values at each site owing to variability in the underlying source signature.

2.4. Atmospheric Chemical Transport Modeling of $\delta^{13}\text{C}(\text{CH}_4)$

We use the global atmospheric chemical transport model Model for Ozone And Related Tracers (MOZART) to simulate atmospheric CH₄ concentrations and $\delta^{13}\text{C}(\text{CH}_4)$ (Emmons et al., 2010). The model is run at $1.9^\circ \times 2.5^\circ$ resolution for 56 vertical levels using the MERRA reanalysis meteorology. The atmosphere is spun up using year 2000 emissions and 1999 meteorology for 100 years at low resolution ($12^\circ \times 11.25^\circ$) followed by 20 years at high resolution. After spin-up, time-varying emissions and dynamics from 2000 to 2012 are used and concentrations analyzed between 2000 and 2012. Fluxes from all source and sink categories and the associated source signature or fractionation factor are presented in the supporting information. All flux magnitudes fall within the range of values reported in Saunois et al. (2016). Global mean $\delta^{13}\text{C}(\text{CH}_4)$ source signatures are broadly similar to those presented in Schwietzke et al. (2016), but some differences are found in ruminants and fossil fuel. The impact of using an alternate database of source signatures is shown in the supporting information. This suite of fluxes and source signatures provide modeled northern hemisphere (NH) and southern hemisphere (SH) mean CH₄ concentrations and $\delta^{13}\text{C}(\text{CH}_4)$ values that are consistent with observed atmospheric observations from 2000 to 2012 (Nisbet et al., 2016).

Two scenarios are modeled in which everything is held the same apart from the wetland source signature: Scenario 1 (S1) uses a globally uniform wetland signature of -62‰ , and Scenario 2 (S2) uses the wetland source signature map derived in this study. The S1 value is chosen to give the same mean area- and flux-weighted signature for the years 2000–2012 as derived from S2 (equation (2)):

$$\bar{\delta} = \frac{\sum f_i A_i \delta_i}{\sum f_i A_i} \quad (2)$$

where f , A , and δ are the flux, area, and source signature of grid cell i and $\bar{\delta}$ is the global mean source signature.

This approach avoids any significant systematic offset in mean atmospheric $\delta^{13}\text{C}(\text{CH}_4)$ arising from the different mean values in the two cases. The mean value of S1 and S2 is similar to the value of -60‰ typically used in previous inverse modeling studies. We assess differences between S1 and S2 in the global mean, spatial distribution, seasonal distribution, and trend during the period 2000 to 2012.

3. Spatially Resolved Wetland Source Signatures

Figure 1 shows the wetland source signature map (masked to show grid cells where wetland fraction from Poulter et al. (2017) is at any time greater than 5%). The mean (flux and area weighted) global source

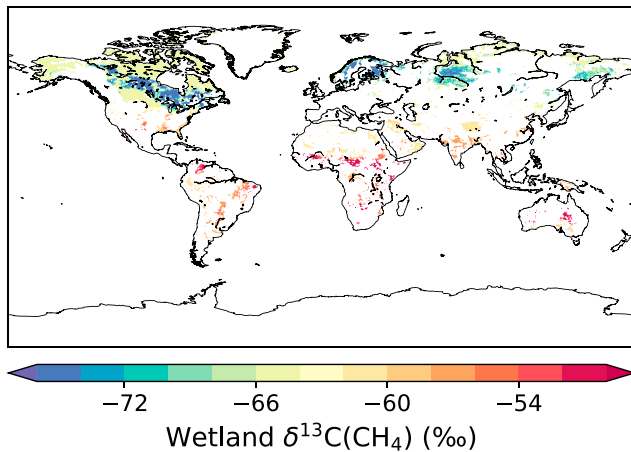


Figure 1. Wetland $\delta^{13}\text{C}(\text{CH}_4)$ source signature map (‰) masked for grid cells where wetland fraction is greater than 5% at any time during the period 2000–2012.

signature from wetlands is -62.0‰ , while the mean boreal signature is -67.8‰ and the mean tropical signature is -56.7‰ . In addition to the latitudinal differences, there is significant regional variability. CH_4 emissions from Canadian and Scandinavian wetlands at approximately -75‰ are significantly more ^{13}C -depleted than the high-latitude mean, while Alaskan wetlands are more ^{13}C -enriched at -65‰ . Regions, such as the Okavango Delta, which host significant C4 papyrus wetlands, are more enriched at -50‰ . Our mean global source signature is similar to the mean microbial signature of $-61.5 \pm 0.6\text{‰}$ reported in Schwietzke et al. (2016), but more negative than the one derived by Feinberg et al. (2018) (approximately -60.5‰), in which a function was fit through samples spanning the tropics and high latitudes. However, the Feinberg et al. (2018) wetland signature function does not capture regional variability in $\delta^{13}\text{C}(\text{CH}_4)$ source signature, which is a primary aim of our study.

To assess the accuracy of this spatially resolved source signature map, we compare simulated and measured atmospheric $\delta^{13}\text{C}(\text{CH}_4)$ at high-latitude and tropical sites using JULES and a suite of additional models

to assess any sensitivity to the flux model (Tables 1 and S2 in the supporting information). For each site and in all models, the mean simulated $\delta^{13}\text{C}(\text{CH}_4)$ value is broadly consistent with the observed values (for reference, S1 would result in atmospheric $\delta^{13}\text{C}(\text{CH}_4)$ of -62‰ at all sites). There is typically a larger uncertainty in the modeled values due to the wetland source variability. The observed wetland source signatures further highlight large regional differences even within similar latitude bands. The largest differences between modeled and observed $\delta^{13}\text{C}(\text{CH}_4)$ values occur in the tropics, suggesting that more studies are needed to either determine fundamental source signatures between C3- and C4-dominated wetlands or to better classify their spatial distribution.

4. Impact on Atmospheric $\delta^{13}\text{C}(\text{CH}_4)$ Variability

We assess the impact on atmospheric $\delta^{13}\text{C}(\text{CH}_4)$ by using the spatially resolved map (S2) presented here rather than a globally uniform wetland signature (S1). This analysis is based on forward modeling, keeping flux fields and source signatures from non-wetland CH_4 sources the same between the two scenarios. We analyze the differences in global mean, spatial distribution, seasonality, and trends during the period 2000 to 2012 between S1 and S2 (Figure 2). While the numbers presented here are specific to this setup of the forward model, the results of the simulation demonstrate the biases that would result in an inversion analysis by

Table 1

Observed Wetland $\delta^{13}\text{C}(\text{CH}_4)$ Signatures (‰) and Modeled Values Using the Source Signature Map Presented in This Study, Fluxes From the JULES Model, and Poulter et al. (2017) Wetland Areas

Site	Measurement type	Observed $\delta^{13}\text{C}(\text{CH}_4)$	Modeled $\delta^{13}\text{C}(\text{CH}_4)$
Alaska	Aircraft	-63.4 ± 3.0^a	-65.1 ± 3.8
Scandinavia	Aircraft	-70.5 ± 2.7^b	-70.0 ± 5.0
East Trout Lake, Canada	Air above surface	-66.8 ± 1.6^b	-68.1 ± 4.2
Fraserdale, Canada	Air above surface	-67.2 ± 1.1^b	-68.8 ± 4.5
Surgut, Siberia	Aircraft	$-70^{c,*}$	-69.9 ± 5.5
Palo Verde, Costa Rica	Air above surface	-53.3 ± 1.7^d	-55.6 ± 3.4
Lake Titicaca, Bolivia	Air above surface	-59.7 ± 1.0^d	-59 ± 4.4
Tor Doone, South Africa	Air above surface	-61.5 ± 0.1^d	-59.7 ± 4.6
Danum Valley, Borneo	Air above surface	-61.5 ± 2.9^d	-60.3 ± 3.9
Mai Po, Hong Kong	Air above surface	-54.6 ± 0.7^d	-56.9 ± 3.8
Kajjansi, Uganda	Air above surface	-53.0 ± 0.4^d	-54.2 ± 3.5

^aUmezawa et al. (2011). ^bFisher et al. (2017). ^cUmezawa et al. (2012). ^dBrownlow et al. (2017).

*Fossil fuel emissions may influence this site, and this signature has applied a correction.

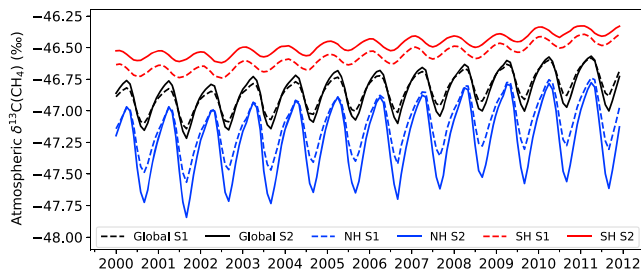


Figure 2. Comparison of atmospheric $\delta^{13}\text{C}(\text{CH}_4)$ (‰) using the spatially resolved wetland source signature distribution (S2, solid lines) versus the common assumption of globally uniform signature (S1, dashed lines). The black lines correspond to the global mean, the blue lines to the northern hemisphere means, and the red lines to the southern hemisphere means.

ical signatures. The interhemispheric difference in $\delta^{13}\text{C}(\text{CH}_4)$ values is 1.4 times larger in S2 (S2-S1 of -0.2‰), and this magnitude is significant compared to the observed interhemispheric (NH-SH) difference of approximately -0.4‰ (Nisbet et al., 2016). The NH seasonal cycle amplitude in $\delta^{13}\text{C}(\text{CH}_4)$ is enhanced by a factor of 1.5 in S2 (S2-S1 of 0.25‰), and this difference is important considering that the observed NH amplitude is $\sim 0.7\text{‰}$. The trend in $\delta^{13}\text{C}(\text{CH}_4)$ is smaller in S2 than S1, due to greater increases in wetland emissions occurring at high latitudes than in the tropical regions in this wetland flux field. The 0.06‰ difference in trend is a significant fraction of the observed change of $\sim 0.2\text{‰}$ that occurred between 2007 and 2014 (Nisbet et al., 2016). This analysis demonstrates that if the uniform $\delta^{13}\text{C}(\text{CH}_4)$ map, S1, were used in an atmospheric inversion, emissions would be derived to compensate for these biases: Emissions would have greater seasonality, a greater spread between NH and SH emissions and slower growth rate than the true emissions. The setup of this forward model is based on commonly used estimates for source and sink fluxes, and quantification of the difference between S2 and S1 is based on forward model configuration. However, the implication is that the biases imparted from inaccurate spatial distribution in $\delta^{13}\text{C}(\text{CH}_4)$ can be of significant size compared to observed values.

In addition to the large-scale differences in global and hemispheric means that are broadly due to latitudinal differences in source signature, there also exist large regional variations in atmospheric $\delta^{13}\text{C}(\text{CH}_4)$ (Figure 3). In Canada and Western Siberia, simulated $\delta^{13}\text{C}(\text{CH}_4)$ is more than 0.5‰ too high without using the spatially resolved map of S2. In contrast, in some South American and African wetland areas, simulated $\delta^{13}\text{C}(\text{CH}_4)$ is 0.5‰ too low. Compared to the surrounding overall latitudinal differences, these regions would still be more

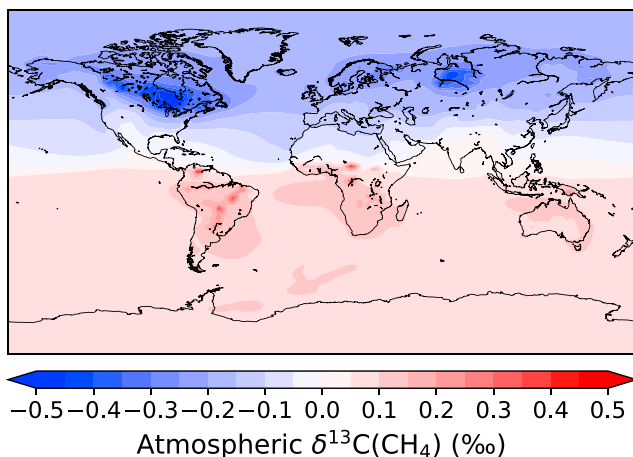


Figure 3. Difference in spatial distribution of atmospheric $\delta^{13}\text{C}(\text{CH}_4)$ (‰) derived using the spatially resolved wetland source signature distribution and a globally uniform signature (S2-S1).

not employing the more accurate spatially resolved map. A direct comparison to observations is out of the scope of this study because we focus on only one component of the global CH_4 budget, whereas uncertainties exist in all components which must be reconciled together.

In both S1 and S2, mean global, NH, and SH CH_4 mole fractions are the same because both scenarios use the same fluxes. The mean global atmospheric $\delta^{13}\text{C}(\text{CH}_4)$ also is similar in both S1 and S2 because we define the mean global flux- and area-weighted $\delta^{13}\text{C}(\text{CH}_4)$ wetland signatures to be the same. Therefore, any differences are solely due to the different spatial distributions in $\delta^{13}\text{C}(\text{CH}_4)$ source signatures. Mean NH and SH $\delta^{13}\text{C}(\text{CH}_4)$ values are ^{13}C -depleted and ^{13}C -enriched, respectively, in S2 compared to S1, by approximately -0.1‰ and 0.1‰ , owing to more ^{13}C -depleted boreal and more ^{13}C -enriched tropi-

cal signatures. In regional atmospheric inversions assimilating $\delta^{13}\text{C}(\text{CH}_4)$ observations, differences of this magnitude would impart a significant bias on retrieved sources.

5. Further Development

There are several areas in which this map could be used to inform future studies. First, the source signature map is a static map and it is likely that wetland source signatures exhibit some seasonal variations, although such temporal differences are expected to be smaller than spatial variations driven by wetland type (Brownlow et al., 2017; Fisher et al., 2017; Hornibrook, 2009). There currently is a scarcity of measurements spanning full annual cycles both in the $\delta^{13}\text{C}(\text{CH}_4)$ flux measurements needed to develop a time-varying map and the atmospheric $\delta^{13}\text{C}(\text{CH}_4)$ data required to validate such a map. Second, we have assimilated the data that currently exist in the literature, but more field studies characterizing $\delta^{13}\text{C}(\text{CH}_4)$ emissions from tropical wetlands are required. Third, we have not included potentially important alterations to wetland signatures based on emission pathways such as trees

(Pangala et al., 2017). Finally, while we have used mean $\delta^{13}\text{C}(\text{CH}_4)$ signatures from each wetland type, there exists variability likely linked to fundamental physical processes such as emission pathway and substrate isotopic composition. When this variability is better quantified, the $\delta^{13}\text{C}(\text{CH}_4)$ source signature map can better incorporate fundamental processes.

6. Conclusions

This work demonstrates the need for accurate, spatially resolved $\delta^{13}\text{C}(\text{CH}_4)$ source signature information to make better use of atmospheric measurements of $\delta^{13}\text{C}(\text{CH}_4)$ for source and sink characterization. We present a spatially resolved wetland $\delta^{13}\text{C}(\text{CH}_4)$ source signature map based on data that have been collected on fundamental differences in $\delta^{13}\text{C}(\text{CH}_4)$ emissions between wetland types. We have validated this map against regional-scale atmospheric observations of wetland $\delta^{13}\text{C}(\text{CH}_4)$ signatures. The $\delta^{13}\text{C}(\text{CH}_4)$ source signature map represents broad features, such as latitudinal gradient, in observed atmospheric $\delta^{13}\text{C}(\text{CH}_4)$, and includes important regional variations. The map provides more accurate regional-scale $\delta^{13}\text{C}(\text{CH}_4)$ source signatures that should be used in atmospheric inversions. We have demonstrated that significant biases would result in flux estimates derived through atmospheric inverse modeling by using a globally uniform wetland $\delta^{13}\text{C}(\text{CH}_4)$ source signature rather than the spatially resolved map presented here.

Acknowledgments

A.G. was funded under a UK Natural Environment Research Council (NERC) Independent Research Fellowship (NE/L010992/1). A.S. was supported by a NERC GW4+ studentship. We acknowledge support for A.G., G.H., and E.C.-P. through NERC grants NE/N016548/1 and NE/N015746/1, for N.G. through the Joint UK BEIS/Defra Met Office Hadley Centre Climate Programme (GA01101), and for B.P. through the Gordon and Betty Moore Foundation grant GBMF5439. NAME footprints were made possible by Bristol's NAME license from the UK Met Office. We thank Rebecca Fisher for valuable discussions on $\delta^{13}\text{C}(\text{CH}_4)$ measurements. The data used in this study are listed in the references, table, and supporting information.

References

- Bartlett, K. B., & Harriss, R. C. (1993). Review and assessment of methane emissions from wetlands. *Chemosphere*, 26(1–4), 261–320. [https://doi.org/10.1016/0045-6535\(93\)90427-7](https://doi.org/10.1016/0045-6535(93)90427-7)
- Bellisario, L. M., Bubier, J. L., Moore, T. R., & Chanton, J. P. (1999). Controls on CH_4 emissions from a northern peatland. *Global Biogeochemical Cycles*, 13(1), 81–91. <https://doi.org/10.1029/1998GB900021>
- Bergamaschi, P., Frankenberg, C., Meirink, J. F., Krol, M., Dentener, F., Wagner, T., et al. (2007). Satellite characterization of atmospheric methane from SCIAMACHY on board ENVISAT: 2. Evaluation based on inverse model simulations. *Journal of Geophysical Research*, 112, D02304. <https://doi.org/10.1029/2006JD007268>
- Bousquet, P., Ciais, P., Miller, J. B., Dlugokencky, E. J., Hauglustaine, D. A., Prigent, C., et al. (2006). Contribution of anthropogenic and natural sources to atmospheric methane variability. *Nature*, 443(7110), 439–443. <https://doi.org/10.1038/nature05132>
- Brownlow, R., Lowry, D., Fisher, R. E., France, J. L., Lanoisellé, M., White, B., et al. (2017). Isotopic ratios of tropical methane emissions by atmospheric measurement. *Global Biogeochemical Cycles*, 31, 1408–1419. <https://doi.org/10.1002/2017GB005689>
- Burkholder, J. B., Sander, S. P., Abbatt, J., Barker, J. R., Huie, R. E., Kolb, C. E., et al. (2015). Chemical kinetics and photochemical data for use in atmospheric studies, Evaluation No. 18, JPL Publication 15–10, Jet Propulsion Laboratory, Pasadena. Retrieved from <http://jpldataeval.jpl.nasa.gov>
- Chanton, J., Crill, P., Bartlett, K., & Martens, C. (1989). Amazon Capims (floating grassmats): A source of ^{13}C enriched methane to the troposphere. *Geophysical Research Letters*, 16(8), 799–802. <https://doi.org/10.1029/GL016i008p00799>
- Chanton, J. P. (2005). The effect of gas transport on the isotope signature of methane in wetlands. *Organic Geochemistry*, 36(5), 753–768. <https://doi.org/10.1016/j.orggeochem.2004.10.007>
- Chasar, L. (2000). Methane concentration and stable isotope distribution as evidence of rhizospheric processes: Comparison of a fen and bog in the Glacial Lake Agassiz Peatland Complex. *Annals of Botany*, 86(3), 655–663. <https://doi.org/10.1006/anbo.2000.1172>
- Comyn-Platt, E., Hayman, G. D., McNorton, J., & Gedney, N. (2018). Monthly global methane emissions from natural wetlands modelled by JULES with dynamic vegetation (1980–2014) v1.0. NERC Environmental Information Data Centre. <https://doi.org/10.5285/6ce61e91-6912-4fe2-a095-12136af86347>
- Coplen, T. B. (2011). Guidelines and recommended terms for expression of stable-isotope-ratio and gas-ratio measurement results. *Rapid Communications in Mass Spectrometry*, 25(17), 2538–2560. <https://doi.org/10.1002/rcm.5129>
- Crill, P. M., Bartlett, K. B., Harriss, R. C., Gorham, E., Verry, E. S., Sebachner, D. I., et al. (1988). Methane flux from Minnesota Peatlands. *Global Biogeochemical Cycles*, 2(4), 371–384. <https://doi.org/10.1029/GB002i004p00371>
- Dlugokencky, E. J., Bruhwiler, L., White, J. W. C., Emmons, L. K., Novelli, P. C., Montzka, S. A., et al. (2009). Observational constraints on recent increases in the atmospheric CH_4 burden. *Geophysical Research Letters*, 36, L18803. <https://doi.org/10.1029/2009GL039780>
- Duddlestone, K. N., Kinney, M. A., Kiene, R. P., & Hines, M. E. (2002). Anaerobic microbial biogeochemistry in a northern bog: Acetate as a dominant metabolic end product. *Global Biogeochemical Cycles*, 16(4), 1063. <https://doi.org/10.1029/2001GB001402>
- Emmons, L. K., Walters, S., Hess, P. G., Lamarque, J.-F., Pfister, G. G., Fillmore, D., et al. (2010). Description and evaluation of the model for ozone and related chemical tracers, version 4 (MOZART-4). *Geoscientific Model Development*, 3(1), 43–67. <https://doi.org/10.5194/gmd-3-43-2010>
- FAO/IIASA/ISRIC/ISSCAS/JRC (2009). Harmonized World Soil Database (version 1.1). FAO, Rome, Italy and IIASA, Laxenburg, Austria.
- Feinberg, A. I., Coulon, A., Stenke, A., Schwietzke, S., & Peter, T. (2018). Isotopic source signatures: Impact of regional variability on the $\delta^{13}\text{C}\text{CH}_4$ trend and spatial distribution. *Atmospheric Environment*, 174, 99–111. <https://doi.org/10.1016/j.atmosenv.2017.11.037>
- Fisher, R. E., France, J. L., Lowry, D., Lanoisellé, M., Brownlow, R., Pyle, J. A., et al. (2017). Measurement of the ^{13}C isotopic signature of methane emissions from northern European wetlands. *Global Biogeochemical Cycles*, 31, 605–623. <https://doi.org/10.1002/2016GB005504>
- Fung, I., John, J., Lerner, J., Matthews, E., Prather, M., Steele, L. P., & Fraser, P. J. (1991). Three-dimensional model synthesis of the global methane cycle. *Journal of Geophysical Research*, 96(D7), 13,033–13,065. <https://doi.org/10.1029/91JD01247>
- Ghosh, A., Patra, P. K., Ishijima, K., Umezawa, T., Ito, A., Etheridge, D. M., et al. (2015). Variations in global methane sources and sinks during 1910–2010. *Atmospheric Chemistry and Physics*, 15(5), 2595–2612. <https://doi.org/10.5194/acp-15-2595-2015>
- Hausmann, P., Sussmann, R., & Smale, D. (2016). Contribution of oil and natural gas production to renewed increase in atmospheric methane (2007–2014): Top-down estimate from ethane and methane column observations. *Atmospheric Chemistry and Physics*, 16(5), 3227–3244. <https://doi.org/10.5194/acp-16-3227-2016>

- Hines, M. E., Duddlestone, K. N., & Kiene, R. P. (2001). Carbon flow to acetate and C₁ compounds in northern wetlands. *Geophysical Research Letters*, 28(22), 4251–4254. <https://doi.org/10.1029/2001GL012901>
- Hornibrook, E. R. C. (2000). Evolution of stable carbon isotope compositions for methane and carbon dioxide in freshwater wetlands and other anaerobic environments. *Geochimica et Cosmochimica Acta*, 64(6), 1013–1027. [https://doi.org/10.1016/S0016-7037\(99\)00321-X](https://doi.org/10.1016/S0016-7037(99)00321-X)
- Hornibrook, E. R. C. (2009). The stable carbon isotope composition of methane produced and emitted from northern peatlands. In *Carbon cycling in northern peatlands, Geophysical Monograph Series* (Vol. 184, pp. 187–203). Washington, DC: American Geophysical Union. <https://doi.org/10.1029/2008GM000828>
- Hornibrook, E. R. C., & Bowes, H. L. (2007). Trophic status impacts both the magnitude and stable carbon isotope composition of methane flux from peatlands. *Geophysical Research Letters*, 34, L21401. <https://doi.org/10.1029/2007GL031231>
- Houweling, S., Dentener, F., & Lelieveld, J. (2000). Simulation of preindustrial atmospheric methane to constrain the global source strength of natural wetlands. *Journal of Geophysical Research*, 105(D13), 17,243–17,255. <https://doi.org/10.1029/2000JD900193>
- JBC/PBL (2014). European Commission, Joint Research Centre (JRC)/Netherlands Environmental Assessment Agency (PBL). Emission Database for Global Atmospheric Research (EDGAR), Release EDGARv4.2 FT2012. Retrieved from <http://edgar.jrc.ec.europa.eu>
- Lansdown, J. M., Quay, P. D., & King, S. L. (1992). CH₄ production via CO₂ reduction in a temperate bog: A source of ¹³C-depleted CH₄. *Geochimica et Cosmochimica Acta*, 56(9), 3493–3503. [https://doi.org/10.1016/0016-7037\(92\)90393-W](https://doi.org/10.1016/0016-7037(92)90393-W)
- Lassey, K. R., Etheridge, D. M., Lowe, D. C., Smith, A. M., & Ferretti, D. F. (2007). Centennial evolution of the atmospheric methane budget: What do the carbon isotopes tell us? *Atmospheric Chemistry and Physics*, 7(8), 2119–2139. <https://doi.org/10.5194/acp-7-2119-2007>
- Manning, A. J., O'Doherty, S., Jones, A. R., Simmonds, P. G., & Derwent, R. G. (2011). Estimating UK methane and nitrous oxide emissions from 1990 to 2007 using an inversion modeling approach. *Journal of Geophysical Research*, 116, D02305. <https://doi.org/10.1029/2010JD014763>
- Matthews, E., & Fung, I. (1987). Methane emission from natural wetlands: Global distribution, area, and environmental characteristics of sources. *Global Biogeochemical Cycles*, 1(1), 61–86. <https://doi.org/10.1029/GB001i001p00061>
- McCarthy, M. C., Boering, K. A., Rice, A. L., Tyler, S. C., Connell, P., & Atlas, E. (2003). Carbon and hydrogen isotopic compositions of stratospheric methane: 2. Two-dimensional model results and implications for kinetic isotope effects. *Journal of Geophysical Research*, 108(D15), 4461. <https://doi.org/10.1029/2002JD003183>
- Melton, J. R., Wania, R., Hodson, E. L., Poulter, B., Ringeval, B., Spahni, R., et al. (2013). Present state of global wetland extent and wetland methane modelling: Conclusions from a model inter-comparison project (WETCHIMP). *Biogeosciences*, 10(2), 753–788. <https://doi.org/10.5194/bg-10-753-2013>
- Mikaloff Fletcher, S. E., Tans, P. P., Bruhwiler, L. M., Miller, J. B., & Heimann, M. (2004). CH₄ sources estimated from atmospheric observations of CH₄ and its ¹³C/¹²C isotopic ratios: 1. Inverse modeling of source processes. *Global Biogeochemical Cycles*, 18, GB4004. <https://doi.org/10.1029/2004GB002223>
- Monteil, G., Houweling, S., Dlugokenky, E. J., Maenhout, G., Vaughn, B. H., White, J. W. C., & Rockmann, T. (2011). Interpreting methane variations in the past two decades using measurements of CH₄ mixing ratio and isotopic composition. *Atmospheric Chemistry and Physics*, 11(17), 9141–9153. <https://doi.org/10.5194/acp-11-9141-2011>
- Murguía-Flores, F., Arndt, S., Ganesan, A. L., Murray-Tortarolo, G. N., & Hornibrook, E. R. C. (2017). Soil Methanotrophy Model (MeMo v1.0): A process-based model to quantify global uptake of atmospheric methane by soil. *Geoscientific Model Development Discussion*, 1–38. <https://doi.org/10.5194/gmd-2017-124>
- Nisbet, E. G., Dlugokenky, E. J., Manning, M. R., Lowry, D., Fisher, R. E., France, J. L., et al. (2016). Rising atmospheric methane: 2007–2014 growth and isotopic shift. *Global Biogeochemical Cycles*, 30, 1356–1370. <https://doi.org/10.1002/2016GB005406>
- Pangala, S. R., Enrich-Prast, A., Basso, L. S., Peixoto, R. B., Bastviken, D., Hornibrook, E. R. C., et al. (2017). Large emissions from floodplain trees close the Amazon methane budget. *Nature*, 552(7684), 230–234. <https://doi.org/10.1038/nature24639>
- Pataki, D. E., Ehleringer, J. R., Flanagan, L. B., Yakir, D., Bowling, D. R., Still, C. J., et al. (2003). The application and interpretation of Keeling plots in terrestrial carbon cycle research. *Global Biogeochemical Cycles*, 17(1), 1022. <https://doi.org/10.1029/2001GB001850>
- Patra, P. K., Houweling, S., Krol, M., Bousquet, P., Belikov, D., Bergmann, D., et al. (2011). TransCom model simulations of CH₄ and related species: Linking transport, surface flux and chemical loss with CH₄ variability in the troposphere and lower stratosphere. *Atmospheric Chemistry and Physics*, 11(24), 12,813–12,837. <https://doi.org/10.5194/acp-11-12813-2011>
- Peregon, A., Maksyutov, S., & Yamagata, Y. (2009). An image-based inventory of the spatial structure of West Siberian wetlands. *Environmental Research Letters*, 4(4), 45014. <https://doi.org/10.1088/1748-9326/4/4/045014>
- Portmann, F. T., Siebert, S., & Döll, P. (2010). MIRCA2000-Global monthly irrigated and rainfed crop areas around the year 2000: A new high-resolution data set for agricultural and hydrological modeling. *Global Biogeochemical Cycles*, 24, GB1011. <https://doi.org/10.1029/2008GB003435>
- Poulter, B., Bousquet, P., Canadell, J. G., Ciais, P., Peregon, A., Saunio, M., et al. (2017). Global wetland contribution to 2000–2012 atmospheric methane growth rate dynamics. *Environmental Research Letters*, 12(9), 94013. <https://doi.org/10.1088/1748-9326/aa8391>
- Quay, P., Stutsman, J., Wilbur, D., Snover, A., Dlugokenky, E., & Brown, T. (1999). The isotopic composition of atmospheric methane. *Global Biogeochemical Cycles*, 13(2), 445–461. <https://doi.org/10.1029/1998GB900006>
- Quay, P. D., King, S. L., Lansdown, J. M., & Wilbur, D. O. (1988). Isotopic composition of methane released from wetlands: Implications for the increase in atmospheric methane. *Global Biogeochemical Cycles*, 2(4), 385–397. <https://doi.org/10.1029/GB002i004p00385>
- Rice, A. L., Butenhoff, C. L., Teama, D. G., Röger, F. H., Khalil, M. A. K., & Rasmussen, R. A. (2016). Atmospheric methane isotopic record favors fossil sources flat in 1980s and 1990s with recent increase. *Proceedings of the National Academy of Sciences of the United States of America*, 113(39), 10,791–10,796. <https://doi.org/10.1073/pnas.1522923113>
- Rigby, M., Manning, A. J., & Prinn, R. G. (2012). The value of high-frequency, high-precision methane isotopologue measurements for source and sink estimation. *Journal of Geophysical Research*, 117, D12312. <https://doi.org/10.1029/2011JD017384>
- Rigby, M., Montzka, S. A., Prinn, R. G., White, J. W. C., Young, D., O'Doherty, S., et al. (2017). Role of atmospheric oxidation in recent methane growth. *Proceedings of the National Academy of Sciences of the United States of America*, 114(21), 5373–5377. <https://doi.org/10.1073/pnas.1616426114>
- Rigby, M., Prinn, R. G., Fraser, P. J., Simmonds, P. G., Langenfelds, R. L., Huang, J., et al. (2008). Renewed growth of atmospheric methane. *Geophysical Research Letters*, 35, L22805. <https://doi.org/10.1029/2008GL036037>
- Saueressig, G., Crowley, J. N., Bergamaschi, P., Brühl, C., Brenninkmeijer, C. A. M., & Fischer, H. (2001). Carbon 13 and D kinetic isotope effects in the reactions of CH₄ with O(¹D) and OH: New laboratory measurements and their implications for the isotopic composition of stratospheric methane. *Journal of Geophysical Research*, 106(D19), 23,127–23,138. <https://doi.org/10.1029/2000JD000120>
- Saunio, M., Bousquet, P., Poulter, B., Peregon, A., Ciais, P., Canadell, J. G., et al. (2016). The global methane budget 2000–2012. *Earth System Science Data*, 8(2), 697–751. <https://doi.org/10.5194/essd-8-697-2016>

- Schaefer, H., Fletcher, S. E. M., Veidt, C., Lassey, K. R., Brailsford, G. W., Bromley, T. M., et al. (2016). A 21st-century shift from fossil-fuel to biogenic methane emissions indicated by $^{13}\text{C}\text{H}_4$. *Science*, 352(6281), 80–84. <https://doi.org/10.1126/science.aad2705>
- Schwietzke, S., Sherwood, O. A., Bruhwiler, L. M. P., Miller, J. B., Etiope, G., Dlugokencky, E. J., et al. (2016). Upward revision of global fossil fuel methane emissions based on isotope database. *Nature*, 538(7623), 88–91. <https://doi.org/10.1038/nature19797>
- Sherwen, T., Schmidt, J. A., Evans, M. J., Carpenter, L. J., Großmann, K., Eastham, S. D., et al. (2016). Global impacts of tropospheric halogens (Cl, Br, I) on oxidants and composition in GEOS-Chem. *Atmospheric Chemistry and Physics*, 16(18), 12,239–12,271. <https://doi.org/10.5194/acp-16-12239-2016>
- Spivakovsky, C. M., Logan, J. A., Montzka, S. A., Balkanski, Y. J., Foreman-Fowler, M., Jones, D. B. A., et al. (2000). Three-dimensional climatological distribution of tropospheric OH: Update and evaluation. *Journal of Geophysical Research*, 105(D7), 8931–8980. <https://doi.org/10.1029/1999JD901006>
- Stevens, C. M., & Engelkemeir, A. (1988). Stable carbon isotopic composition of methane from some natural and anthropogenic sources. *Journal of Geophysical Research*, 93(D1), 725–733. <https://doi.org/10.1029/JD093iD01p00725>
- Still, C. J., Berry, J. A., Collatz, G. J., & DeFries, R. S. (2003). Global distribution of C_3 and C_4 vegetation: Carbon cycle implications. *Global Biogeochemical Cycles*, 17(1), 1006. <https://doi.org/10.1029/2001GB001807>
- Tarnocai, C., Kettles, I. M., & Lacelle, B. (2000). Peatlands of Canada (1:6 500 000 Map, Open File 3834). Geological Survey of Canada.
- Turetsky, M. R., Kotowska, A., Bubier, J., Dise, N. B., Crill, P., Hornibrook, E. R. C., et al. (2014). A synthesis of methane emissions from 71 northern, temperate, and subtropical wetlands. *Global Change Biology*, 20(7), 2183–2197. <https://doi.org/10.1111/gcb.12580>
- Turner, A. J., Frankenberg, C., Wennberg, P. O., & Jacob, D. J. (2017). Ambiguity in the causes for decadal trends in atmospheric methane and hydroxyl. *Proceedings of the National Academy of Sciences of the United States of America*, 114(21), 5367–5372. <https://doi.org/10.1073/pnas.1616020114>
- Tyler, S. C., Zimmerman, P. R., Cumberbatch, C., Greenberg, J. P., Westberg, C., & Darlington, J. P. E. C. (1988). Measurements and interpretation of $\delta^{13}\text{C}$ of methane from termites, rice paddies, and wetlands in Kenya. *Global Biogeochemical Cycles*, 2(4), 341–355. <https://doi.org/10.1029/GB002i004p00341>
- Umezawa, T., Aoki, S., Kim, Y., Morimoto, S., & Nakazawa, T. (2011). Carbon and hydrogen stable isotopic ratios of methane emitted from wetlands and wildfires in Alaska: Aircraft observations and bonfire experiments. *Journal of Geophysical Research*, 116, D15305. <https://doi.org/10.1029/2010JD015545>
- Umezawa, T., Machida, T., Ishijima, K., Matsueda, H., Sawa, Y., Patra, P. K., et al. (2012). Carbon and hydrogen isotopic ratios of atmospheric methane in the upper troposphere over the Western Pacific. *Atmospheric Chemistry and Physics*, 12(17), 8095–8113. <https://doi.org/10.5194/acp-12-8095-2012>
- van der Werf, G. R., Randerson, J. T., Giglio, L., van Leeuwen, T. T., Chen, Y., Rogers, B. M., et al. (2017). Global fire emissions estimates during 1997–2016. *Earth System Science Data*, 9(2), 697–720. <https://doi.org/10.5194/essd-9-697-2017>
- Velders, G. J. M. (1995). Description of the RIVM 2-dimensional strato-sphere model, RIVM Rep. 722201002, Bilthoven, Netherlands.
- Warwick, N. J., Cain, M. L., Fisher, R., France, J. L., Lowry, D., Michel, S. E., et al. (2016). Using $\delta^{13}\text{C}\text{-CH}_4$ and $\delta\text{D}\text{-CH}_4$ to constrain Arctic methane emissions. *Atmospheric Chemistry and Physics*, 16(23), 14,891–14,908. <https://doi.org/10.5194/acp-16-14891-2016>
- Whiticar, M., & Schaefer, H. (2007). Constraining past global tropospheric methane budgets with carbon and hydrogen isotope ratios in ice. *Philosophical Transactions of the Royal Society A: Mathematical, Physical and Engineering Sciences*, 365(1856), 1793–1828. <https://doi.org/10.1098/rsta.2007.2048>
- Worden, J. R., Bloom, A. A., Pandey, S., Jiang, Z., Worden, H. M., Walker, T. W., et al. (2017). Reduced biomass burning emissions reconcile conflicting estimates of the post-2006 atmospheric methane budget. *Nature Communications*, 8(1), 2227. <https://doi.org/10.1038/s41467-017-02246-0>
- Yan, X., Akiyama, H., Yagi, K., & Akimoto, H. (2009). Global estimations of the inventory and mitigation potential of methane emissions from rice cultivation conducted using the 2006 Intergovernmental Panel on Climate Change Guidelines. *Global Biogeochemical Cycles*, 23, GB2002. <https://doi.org/10.1029/2008GB003299>